https://doi.org/10.3311/PPee.39807

Periodica Polytechnica Electrical Engineering and Computer Science, 69(3), pp. 215–225, 2025

Enhanced Fuzzy-Power Control for WECS based on Variable Wind Speed-Driven DFIG Using SVM Strategy under Sub- and Super-synchronous Operating Modes

Fayssal Amrane[1*], Hichem Itouchene[2]

[1] LAS Research Laboratory, LEPCI Laboratory, Electrotechnic Department, Setif-1 University Ferhat ABBAS, 19000 Setif, Algeria
[2] Université de Bejaia, Faculté de Technologie, Laboratoire de Technologie Industrielle et de l'Information (LTII), 06000 Bejaia, Algeria
[*] Corresponding author, e-mail: amrane_fayssal@univ-setif.dz

Received: 07 January 2025, Accepted: 12 August 2025, Published online: 01 September 2025

Abstract

This paper presents an efficient stator power control algorithm for a grid-connection wind turbine system based on a doubly fed induction generator (DFIG) operating under variable wind speed conditions. The proposed approach focuses on controlling the stator power of the DFIG under varying operating conditions. In order to extract maximize wind power extraction, the stator-side power factor is maintained at unity through maximum power point tracking (MPPT). An advanced fuzzy-type controller, known as Type-2 Fuzzy logic control (T2-FLC), is proposed to regulate the rotor's direct and quadrature currents. Simulation results obtained in the MATLAB/Simulink environment demonstrate that the T2-FLC controller offers robust performance, superior dynamic response, and enhanced operational efficiency for the wind energy and drive applications in steady-states conditions.

Keywords

doubly fed induction generator, wind energy, maximum power point tracking, space vector modulation, type-2 fuzzy logic control

1 Introduction

The wind energy (WE) is one of the most promising technologies in the renewable energy sector [1, 2]. The rapid development of wind energy is largely attributed to its adaptability across diverse geographical areas and its relatively competitive costs compared to other energy sources [3]. As illustrated in Fig. 1, global energy investments from 2019 to 2023 reflect a clear shift toward renewables, which surpassed 600 billion USD in 2023, making it the most funded energy sector. By contrast, investments in fossil fuels remained below 200 billion USD annually, while grids and storage systems saw steady growth, reaching approximately 300 billion USD by 2023. Nuclear energy investments, though the lowest, showed slight but consistent growth, remaining under 100 billion USD throughout the period. This data underscores a global trend prioritizing renewable energy and the modernization of energy systems, marking a decisive shift away from fossil fuels.

Among renewable energy technologies, wind turbines equipped with doubly fed induction generators (DFIG) have gained significant attention due to their variable-speed capabilities [4–6]. Many installed wind turbines today rely on doubly fed induction machines (DFIM), but earlier designs often avoided converters by directly connecting the machines to the grid. This direct connection, while simpler, constrained operational speeds and reduced efficiency at high wind speeds. In contrast, DFIG-based wind turbines enhance system dynamics by enabling variable-speed operation. A DFIG comprises a wound rotor induction generator (WRIG) with stator windings directly connected to a three-phase power grid, while the rotor windings are interfaced with a bidirectional back-to-back IGBT frequency converter [7]. The Fig. 2 presents a schematic diagram of a variable-speed wind turbine system with a DFIG.

The power vector control (PVC) is one of the most applications of DFIG based on the proportional-integral (PI) controller [8]. Control strategies of DFIG have been discussed in literatures; direct power control (DPC) [9], model predictive direct power control (MPDPC) [10, 11], sliding mode direct power control [12], second-order sliding mode control [13] and backstepping control [14].

Cite this article as: Amrane, F., Itouchene, H. "Enhanced Fuzzy-Power Control for WECS based on Variable Wind Speed-Driven DFIG Using SVM Strategy under Sub- and Super-synchronous Operating Modes", Periodica Polytechnica Electrical Engineering and Computer Science, 69(3), pp. 215–225, 2025. https://doi.org/10.3311/PPee.39807

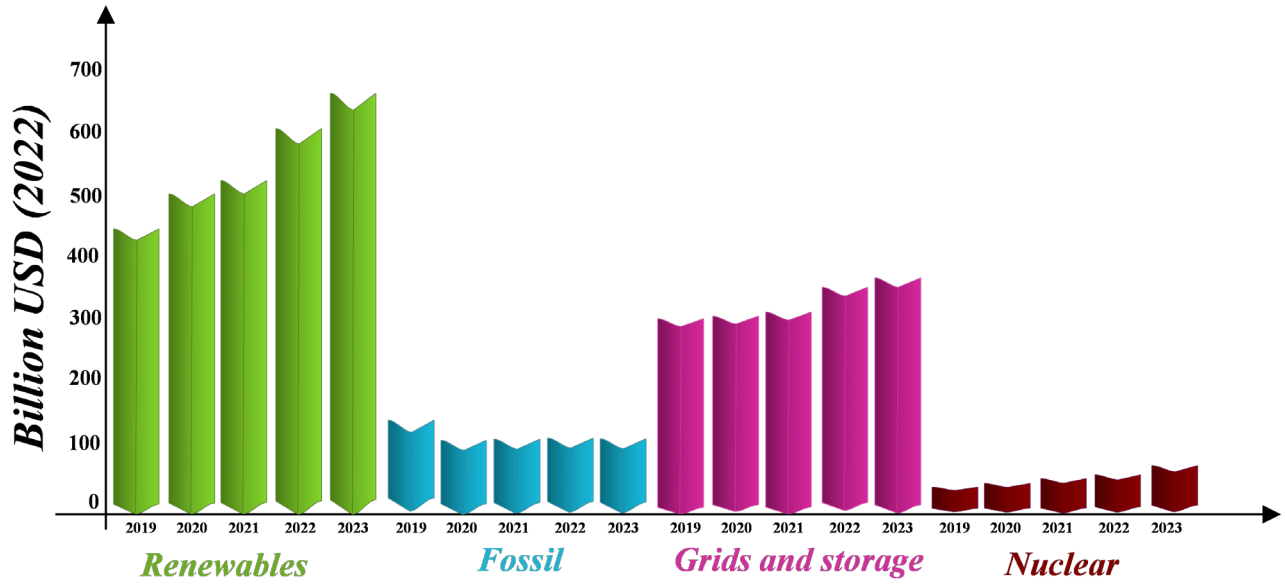

Fig. 1 Global energy investment by sector (2019–2023)

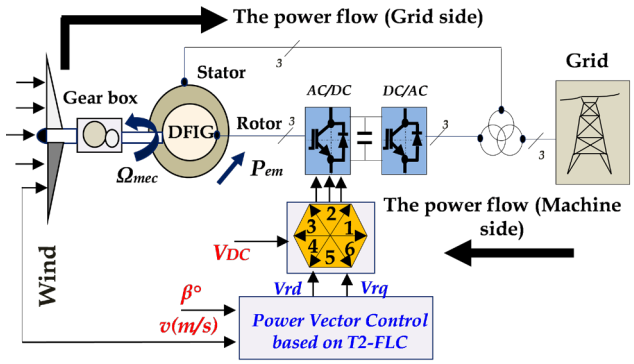

Fig. 2 Control scheme based on DFIG power control

In [1] the authors have proposed a robust control strategy based on an integral backstepping controller (INT-BCS-Control) leveraging the Lyapunov function to enhance the performance of doubly fed induction generator (DFIG) wind turbines operating in Sup/Super Synchronous mode.

The primary aim is to achieve the decoupling of active and reactive power while ensuring high robustness, thus turbines within grid-connected systems. In [5] the authors address the limitations of improving the performance and reliability of DFIG wind conventional PI controllers in handling variations in DFIG parameters and wind speed by applying sliding mode theory. Two robust nonlinear control techniques, Conventional Sliding Mode Control (C-SMC) and Third Order Sliding Mode Control (3O-SMC), were implemented to regulate stator active and reactive powers. However, both exhibited chattering due to discontinuous signals. To mitigate this, the authors introduced an advanced Variable Gain Super Twisting Algorithm (VGSTA). In [15] the authors have proposed tow topologies based in Type-1 fuzzy logic controller (*T1-FLC*) and Type-2 fuzzy logic controller (*T2-FLC*) to achieve high performance sensorless drive in both transient and steady state conditions.

In [16], stator active and reactive powers are controlled via PI regulation loops to control (P_s, Q_s) and (I_{rd}, I_{rq}) respectively, due to the performance limitations of the classical control which depends on accurate knowledge of machine parameters such as stator and rotor resistances and inductances which may degrade according to physical conditions, some drawbacks appears such as; remarkable overshoot, high value of THD stator current, important power error, remarkable response time and bad tracking power reference in case of sudden variation of wind speed. In [17], the authors introduced a control strategy that modifies the Super-Twisting Control approach by incorporating adaptive gains, specifically applied to a grid-connected wind power system using a DFIG. This method was compared with the traditional super-twisting control, and the results showed that the proposed technique reduces the control effort and simplifies the sliding mode formulation, even in the presence of disturbances like parameter variations and fluctuating wind speeds. In [18], the authors investigated adaptive second-order sliding mode control techniques aimed at maximizing the wind energy extraction in a WECS. Their modelling and simulation results demonstrated the robustness and relative simplicity of the control method.

The main contribution of this paper is the development and validation of a robust adaptive T2-FLC

algorithm, aimed at optimizing the performance of a DFIG-based WECS. This advanced control strategy is meticulously designed to ensure efficient and stable operation under varying and unpredictable wind conditions. A key aspect of this research is the integration of a MPPT strategy, which plays a pivotal role in maximizing the energy harnessed from the wind turbine. The proposed MPPT algorithm dynamically adjusts the operating conditions, enabling the system to respond effectively to sudden and erratic changes in wind speed. This dynamic adaptation not only enhances energy capture but also improves the overall reliability and efficiency of the WECS. To ensure seamless integration with the power grid, the control algorithm incorporates a mechanism to maintain a unity power factor at the stator terminals. By regulating the stator reactive power to zero, the system effectively eliminates any reactive power exchange with the grid. As a result, the DFIG-based WECS exclusively transfers active power from the stator to the grid, thereby improving energy efficiency and ensuring better grid compatibility.

This paper is organized as follows: Firstly, the modeling of the turbine is presented in Section 2. In Section 3, the mathematical model of the DFIG is provided. Section 4 focuses on the active and reactive power control of the DFIG, which is based on the orientation of the stator flux vector along the d-axis. Additionally, the modeling of the proposed Type-2 Fuzzy Logic approach is established to control the rotor currents using a two-level inverter (AC-DC). In Section 5, the simulation results are presented and discussed. Finally, the conclusions of the reported work are provided.

2 Mathematical model of WT

The input power of the WT is given by [4, 19].

$$P_v = \frac{1}{2}\cdot\rho\cdot S_w\cdot v^3, \tag{1}$$

where ρ is the air density; S_w is the WT blade swept area; v is the wind speed.

The mechanical power output of a WT is given by:

$$P_m = C_p\cdot P_v = \frac{1}{2}\cdot C_p\cdot\rho\cdot S_w\cdot v^3, \tag{2}$$

where: The power coefficient (C_p) represents the WT's power conversion efficiency. C_p is a non-linear function of the Tip Speed Ratio (*TSR* or λ) and the blade angle ($B°$)

TSR is given by:

$$\lambda = \frac{R\cdot\Omega_t}{v}, \tag{3}$$

where: R is the blade radius, and Ω_t is the angular speed of the turbine.

The expression for $C_p(\lambda,\beta)$ can be described as [3, 16]:

$$C_p(\lambda,\beta) = \left(0.5-0.0167\cdot(\beta-2)\right)\cdot\sin\left[\frac{\pi\cdot(\lambda+0.1)}{18.5-0.3\cdot(\beta-2)}\right]-0.00184\cdot(\lambda-3)\cdot(\beta-2) \tag{4}$$

The MPPT strategy without wind speed control is illustrated in Fig. 3. In this case, the P_s^* (stator power reference) is calculated by multiplying the MPPT's output (the mechanical speed Ω_{mec}) by the electromagnetic torque T_{em}^*, which results in $P_s^* = \Omega_{mec}\cdot T_{em}^*$.

By using MATLAB/Simulink® to show the three-dimensional (3D) characteristic of C_p versus *TSR* and pitch angles ($B°$), as shown in Fig. 4, the main aim of the MPPT strategy is to adapt the turbine speed to the wind speed in order to maximize the converted power. This will improve its energy efficiency and integration with the grid.

3 Mathematical model of DFIG

The selected generator for the conversion of wind energy is a DFIG. The modeling of the DFIG is derived from the

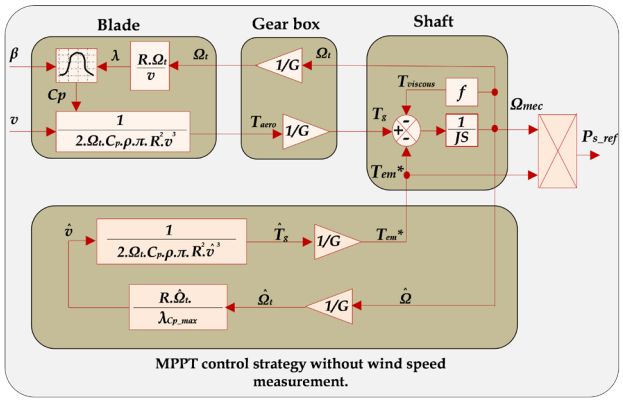

Fig. 3 MPPT strategy without wind speed control

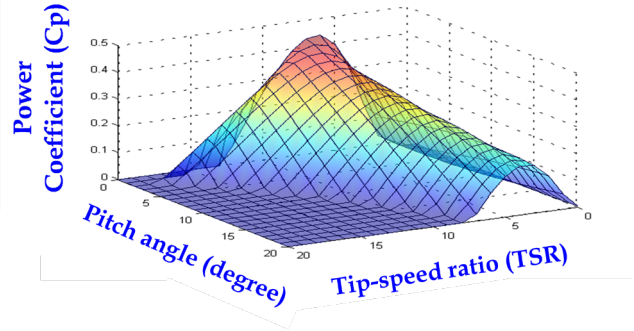

Fig. 4 3D Power coefficient vs. TSR and Pitch angle degree

induction machine model using Park the two-phase reference frame. The overall electrical state transformation is represented by the following equations [4, 20–24]:

$$V_{sd} = R_s \cdot i_{sd} + \frac{d}{dt}\Phi_{sd} - \omega_s \cdot \Phi_{sq} \tag{5}$$

$$V_{sq} = R_s \cdot i_{sq} + \frac{d}{dt}\Phi_{sq} + \omega_s \cdot \Phi_{sd} \tag{6}$$

$$V_{rd} = R_r \cdot i_{rd} + \frac{d}{dt}\Phi_{rd} - (\omega_s - \omega) \cdot \Phi_{rq} \tag{7}$$

$$V_{rq} = R_r \cdot i_{rq} + \frac{d}{dt}\Phi_{rq} + (\omega_s - \omega) \cdot \Phi_{rd} \tag{8}$$

$$\Phi_{sd} = L_s \cdot i_{sd} + L_m \cdot i_{rd} \tag{9}$$

$$\Phi_{sq} = L_s \cdot i_{sq} + L_m \cdot i_{rq} \tag{10}$$

$$\Phi_{rd} = L_r \cdot i_{rd} + L_m \cdot i_{sd} \tag{11}$$

$$\Phi_{rq} = L_r \cdot i_{rq} + L_m \cdot i_{sq} \tag{12}$$

The electromagnetic torque is given by:

$$C_e = P \cdot L_m \cdot \left(I_{rd} \cdot I_{sq} - I_{rq} \cdot I_{sd}\right) \tag{13}$$

And its associated motion equations are:

$$T_e - T_r = J \cdot \frac{d}{dt}\Omega + f \cdot \Omega \tag{14}$$

$$J = \frac{J_{\text{turbine}}}{G^2} + J_g, \tag{15}$$

where: Φ_{sd}, Φ_{sq} are stator flux components, Φ_{rd}, Φ_{rq} are rotor flux components, V_{sd}, V_{sq} are stator voltage components, V_{rd}, V_{rq} are rotor voltage components. R_s, R_r are stator and rotor resistances, L_s, L_r are stator and rotor inductances, L_m is mutual inductance, σ is leakage factor, P is number of pole pairs, f is the friction coefficient, T_r is the load torque, J is total inertia in DFIG's rotor, Ω is mechanical speed, g is the slip, and G is gain of gearbox.

4 Vector power control (VPC) based on T2-FLC

In this section, the DFIG model is described by the following state equations in the synchronous reference frame, where the d-axis is aligned with the stator flux vector ($\Phi_{sd} = \Phi_s$) and ($\Phi_{sq} = 0$), as shown in Fig. 5 [19–23].

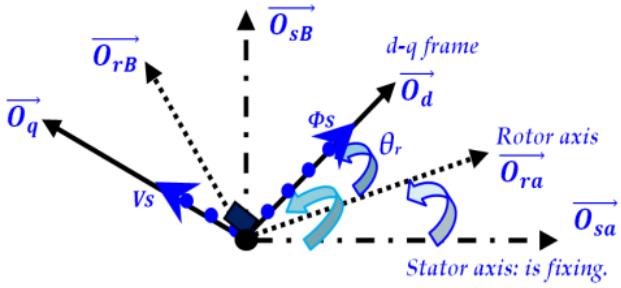

Fig. 5 Stator and rotor flux vectors in the synchronous *d-q* frame

By neglecting resistances of the stator phases, the stator voltage can be written as:

$$V_{sq} = 0 \quad and \quad V_{sq} = V_s \cong \omega_s \cdot \Phi_s \tag{16}$$

We lead to an uncoupled power control, where the transversal component irq of the rotor current controls the active power. The reactive power is determined by the direct component ird. The simplified mathematical model of the DFIG is illustrated in Fig. 6.

$$P_s = -V_s \cdot \frac{L_m}{L_s} \cdot i_{rq} \tag{17}$$

$$Q_s = \frac{V_s^2}{\omega_s \cdot L_s} - V_s \cdot \frac{L_m}{L_s} \cdot i_{rd} \tag{18}$$

The arrangement of the equations provides the expressions for the voltages in terms of the rotor currents:

$$V_{rd} = R_r \cdot i_{rd} + \left(L_r - \frac{L_m^2}{L_s}\right) \cdot \frac{di_{rd}}{dt} - g \cdot \omega_s \cdot \left(L_r - \frac{L_m^2}{L_s}\right) \cdot i_{rq} \tag{19}$$

$$\begin{aligned} V_{rq} &= R_r \cdot i_{rq} + \left(L_r - \frac{L_m^2}{L_s}\right) \cdot \frac{di_{rq}}{dt} \\ &+ g \cdot \omega_s \cdot \left(L_r - \frac{L_m^2}{L_s}\right) \cdot i_{rd} + g \cdot \frac{L_m \cdot V_s}{L_s} \end{aligned} \tag{20}$$

$$i_{rd} = -\frac{1}{\sigma \cdot \tau_r} \cdot i_{rd} + g \cdot \omega_s \cdot i_{rq} + \frac{1}{\sigma \cdot L_r} \cdot V_{rd} \tag{21}$$

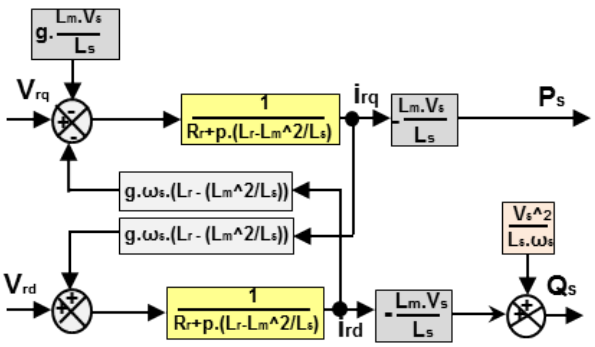

Fig. 6 The simplified mathematical model of the DFIG

$$i_{rq} = -\frac{1}{\sigma}\left(\frac{1}{\tau_r} + \frac{L_m^2}{L_s \cdot T_s \cdot L_r}\right) \cdot i_{rq} - g \cdot \omega_s \cdot i_{rd} + \frac{1}{\sigma \cdot L_r} \cdot V_{rq} \quad (22)$$

With:

$$T_r = \frac{L_r}{R_r}; \quad T_s = \frac{L_s}{R_r}; \quad \sigma = 1 - \frac{L_m^2}{L_s \cdot L_r} \quad (23)$$

The voltage vectors produced by a three-phase PWM inverter divide the space vector plane into 6 sectors, as shown in Fig. 7 [4, 21]. In each sector, every voltage vector is synthesized by the basic space voltage vector of the 2 sides of the sector and one zero vector. For example, in the first sector, $V_{\alpha\beta}$ is a synthesized voltage space vector and can be written as:

$$\vec{V}_{\alpha\beta} = \frac{T_1}{T_S} \cdot \vec{V}_1 + \frac{T_2}{T_S} \cdot \vec{V}_2 \quad (24)$$

4.1 Design of T2-FLC

Fuzzy inference is a method that interprets the values in the input vector and, based on user-defined rules, assigns values to the output vector. Using the GUI editors and viewers in the Fuzzy Logic Toolbox (Fig. 8(a)), the user can build the rule set (Fig. 8(b)), define the membership functions (Fig. 8(c)), and analyze the behavior of the fuzzy inference system (FIS) (Fig. 8(d)). The T2-FLC used in this work has two inputs and one output. The membership functions are defined in Figs. 9(a) and 9(b), in this work the T2-FLC has two (02) inputs and 01 input.

Each rule has the form: if "Input-1" is "Fuzzy-Set" and "Input-2" is "Fuzzy-Set" then "Output" is "Fuzzy-Set". Knowing that: N: negative, P: positive, B: big, M: medium, S: small, and 2: type-2. G1, G2 and G3 are the gains of T2-FLC controller.

The fuzzy rule base consists of a collection of linguistic rules of the form [22]:

Rule 1: if $S_{1,2}$ is NB2, and $S_{1,2}$ is NB2 then $dU_{1,2}$ is NB2
Rule 2: if $S_{1,2}$ is NM2, and $S_{1,2}$ is NB2 then $dU_{1,2}$ is NB2
Rule 3: if $S_{1,2}$ is NS2, and $S_{1,2}$ is NG2 then $dU_{1,2}$ is NS2

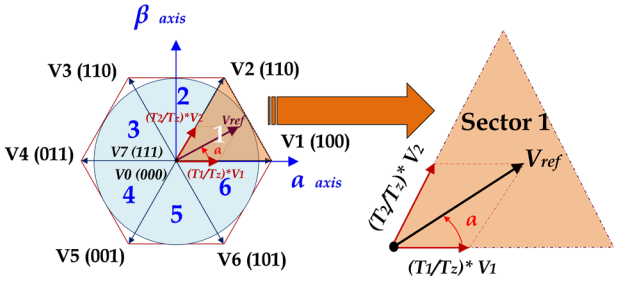

Fig. 7 Diagram of voltage space vectors in α-β plan

.
.

Rule 49: if $S_{1,2}$ is PB2, and $S_{1,2}$ is PB2 then $dU_{1,2}$ is PB2.

These inferences can be explained in more detail, as shown in Table. 1 [22]. The equivalent Simulink model of the proposed T2-FLC for adjusting rotor currents is presented in Fig. 9. The proposed T2FLC for a DFIG rotor currents control is shown in Fig. 10.

5 Simulation results and discussion

The DFIG used in this work is a 4kW machine, with its nominal parameters listed in Table A1, while the wind turbine is a 4.5 kW unit, with its parameters provided in Table A2.

The proposed system is validated under the MPPT strategy by maintaining the stator reactive power at 0 Var to ensure unity power factor (PF = 1). Additionally, the *SVM* approach is employed to ensure a fixed switching frequency for the inverter's IGBTs

This section explains the operating modes of a DFIG using the variation in sinusoidal rotor currents. Fig. 11 demonstrates the rotor's measured current behavior as the speed fluctuates around 1500 rpm (synchronous region). Both transitions from sub-synchronous to super-synchronous modes and vice versa are analyzed. The rotor currents mirror the random wind speed pattern because they are controlled based on the slip angle ($\theta_{slip} = \int_0^t(\omega_{slip} = \omega_s - \omega_r)$ dt + θ_{s0} where $\omega_s = 2\pi f$, and $\omega_r = P{\cdot}\Omega_{mec}$). The slip angle is directly influenced by the DFIG rotor speed, which correlates to the wind speed derived from the *MPPT* strategy. Note that the rotor currents (I_{rabc}) are scaled by a factor of 80 ($\rightarrow I_{rabc}{\cdot}80$). The direction of rotor power flow depends on the operating mode: during the transition from sub-synchronous to super-synchronous, the rotor draws power from the grid, whereas in the reverse transition, the rotor supplies power to the grid through the back-to-back converter. Table 2 summarizes the DFIG speed values under these operating conditions.

Fig. 12(a) presents the stator active and reactive powers, along with their reference profiles, using proposed control for a 0° pitch angle (β° = 0°). It can be seen that the measured powers (P_s and Q_s) follow theirs references exactly, despite the sudden variation of wind speed during steady states. Fig. 12(b) illustrates the behavior of P_s in case of different values of pitch angle (B° = 0°, 1°, 1.5°, 2° and 2.05°).

It is clear that the maximum wind power is reached at B = 0° (*black color*). In the same context, there is an inverse proportionality between the value of angle pitch B° and the extracted power. Fig. 12(c) shows the behavior of Q_s for

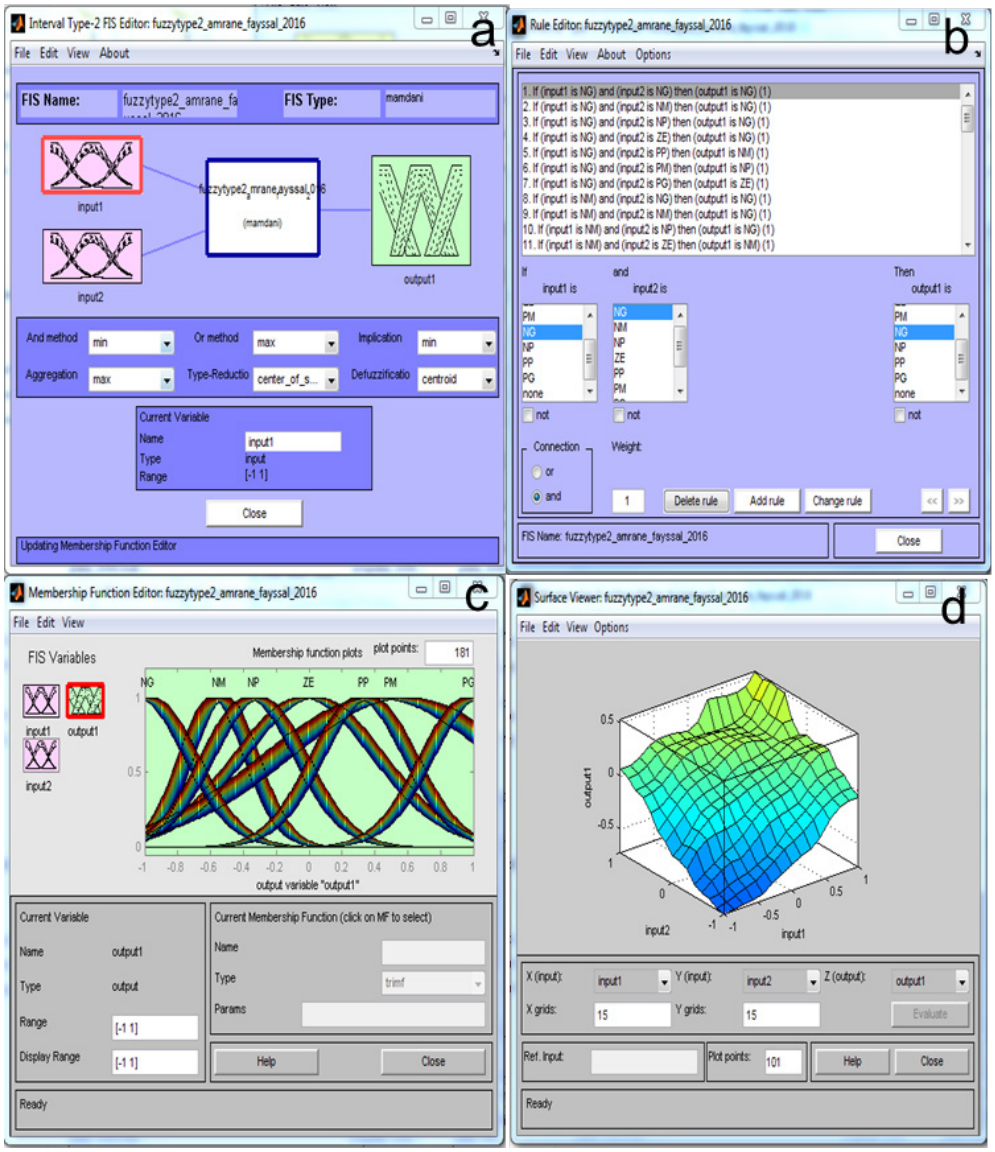

Fig. 8 (a) Membership function editor of the T2-FL toolbox; (b) rule editor of the T2-FL toolbox; (c) 2Inputs, 1-Output Membership function editor of the T-2FL Toolbox; (d) surface viewer of the T2-FL toolbox

different pitch angle (B° = 0°, 1°, 1.5°, 2° and 2.05°). It is clear that for different pitch angles, Q_s remains at the zero level, with a small power error (ΔP_s $\Delta Q_s \approx \pm$ 150 W Var) between 0.75 s and 0.9 s. This is because in this period, P_s reaches its maximum value at $\beta° = 0°$, meaning that the maximum power is extracted, and the power factor remains at unity (PF = 1), despite the sudden variation in wind speed.

In this proposed system, we used a random wind speed, as shown in Fig. 12(d), with a maximum value reaching 15.5 m/s at 0.8 s. It is obvious that the generator speed follows the same waveform as the wind speed. It is important to describe the generator speed (as shown in Fig. 12(e)) taking in into consideration the synchronous speed (1500 rpm). The two, zone "1" and "2", as shown in Fig. 12(e), represent the Sub- and Super-synchronous mode, respectively. That means that the Sub-synchronous mode operates at speeds below 1500 rpm (where the rotor absorbs power: max +30%.Ps) while the Super-synchronous mode operates at speeds above 1500 rpm (where the rotor delivers the power to grid: max −30%.Ps). Fig. 12(f) illustrates the behavior of the power coefficient C_p during the sudden variation in wind speed, maintaining the maximum power (C_p = 0.4785). The behavior of slip during the Sub-synchronous and Super-synchronous operating modes is represented in Fig. 12(g). The slip is depends on the synchronous speed ns ($g = n_s - (n/n_s)$), where, n_s = 1500 rpm and, n being the rotor shaft speed, which is dependent on wind speed. The rotor currents are illustrated in Fig. 12(h). It can be seen the behavior of the three phase's rotor currents varies during the slip variation.

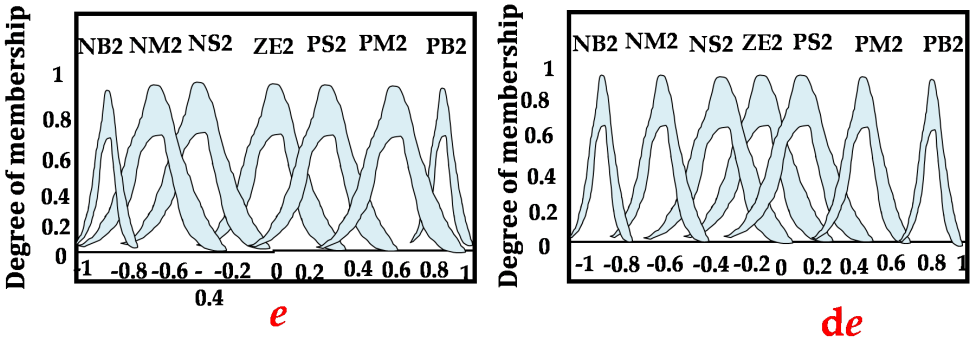

(a)

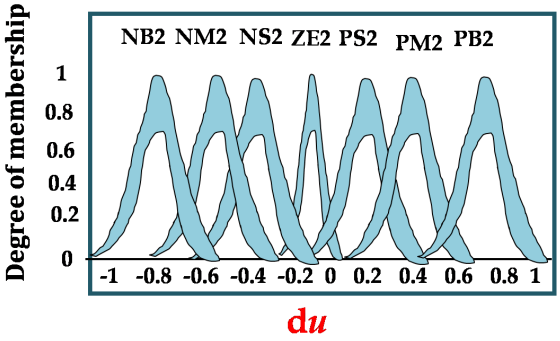

(b)

Fig. 9 T2-FLC Membership functions, (a) two inputs, and (b) one input

Table 1 Type-2 fuzzy inference table

Input	$dU_{1,2}$	$dS_{1,2}$						
		NB2	NM2	NS2	EZ2	PS2	PM2	PB2
$S_{1,2}$	NB2	NB2	NB2	NB2	NM2	NS2	NS2	EZ2
	NM2	NB2	NM2	NM2	NM2	NS2	EZ2	PS2
	NS2	NB2	NM2	NS2	NS2	EZ2	PS2	PM2
	EZ2	NB2	NM2	NS2	EZ2	PS2	PM2	PM2
	PS2	NM2	NS2	EZ2	PS2	PS2	PM2	PB2
	PM2	NS2	EZ2	PS2	PM2	PM2	PM2	PB2
	PB2	EZ2	PS2	PS2	PM2	PB2	PB2	PB2

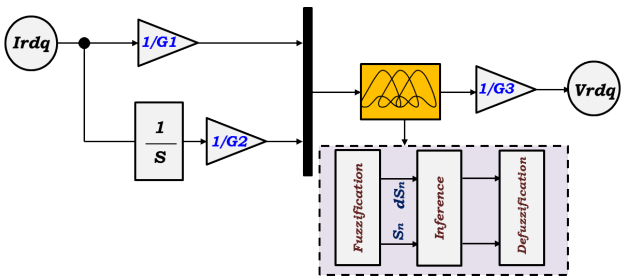

Fig. 10 The Simulink model of T2-FLC for rotor currents

The existence of overshoot, the THD of stator and rotor currents, and the values of active and reactive power errors are mentioned in Table 3. Table 4 presents a comparative analysis between the proposed control method and other recently published control technologies, highlighting the advantages and limitations of the proposed method [5, 7, 19, 25–31].

6 Work limitation

The work presented in this paper demonstrates the effectiveness of a T2-FLC for controlling a WECS based on a Doubly Fed Induction Generator. However, several limitations should be noted. First, the study assumes ideal conditions, such as perfect MPPT and unity power factor, which may not always hold true in real-world scenarios. The impact of disturbances like grid faults or unexpected variations in wind speed has not been fully explored.

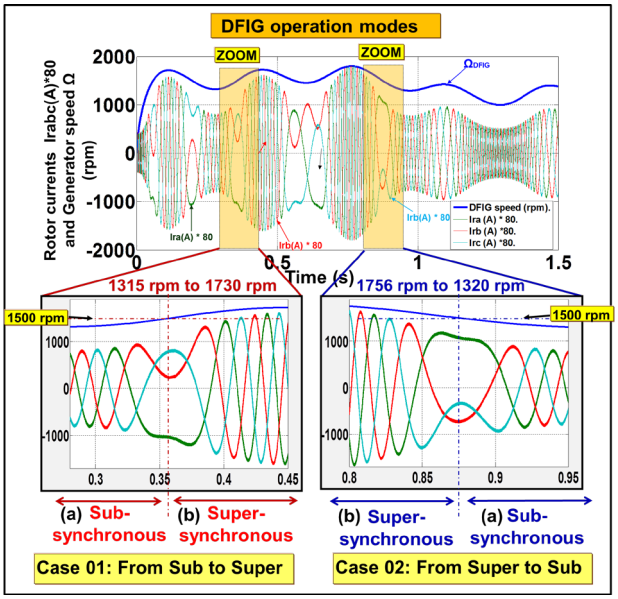

Fig. 11 Simulations results of DFIG operation modes: (a) sub-synchronous, (b) super-synchronous

Table 2 DFIG operation modes parameters

Cases:	DFIG operation mode
Case 01	From Sub to Super-synchronous speed: → 1315 to 1730 rpm
Case 02	From Super to Sub-synchronous speed: → 1756 to 1320 rpm

Table 3 Wind system performances

Criteria	Proposed control based on T2FLC
Overshoot	Neglected
Stator Current's THD	0.60%.
Rotor Current's THD	01.47%.
Power's error	+/− 150 (W_Var).

Additionally, while the T2-FLC provides excellent performance in the simulations, the system's robustness to real-time factors, such as thermal effects, electromagnetic interference, and practical control delays, has not been tested. The work also relies on a simplified wind speed profile, which may not fully capture the complexities of actual wind conditions, such as turbulence and gusts. Moreover, the scalability of the system to higher power ratings is not discussed which limits the applicability to large commercial wind turbines.

The simulation results, while promising, lack real-world experimental validation, which could offer a better understanding of the controller's practical performance. Furthermore, the study does not explore the potential benefits of comparing the T2-FLC with other advanced control strategies like Model Predictive Control (MPC) or Adaptive Neural Network Controllers, which could offer insights into the relative advantages of the proposed approach.

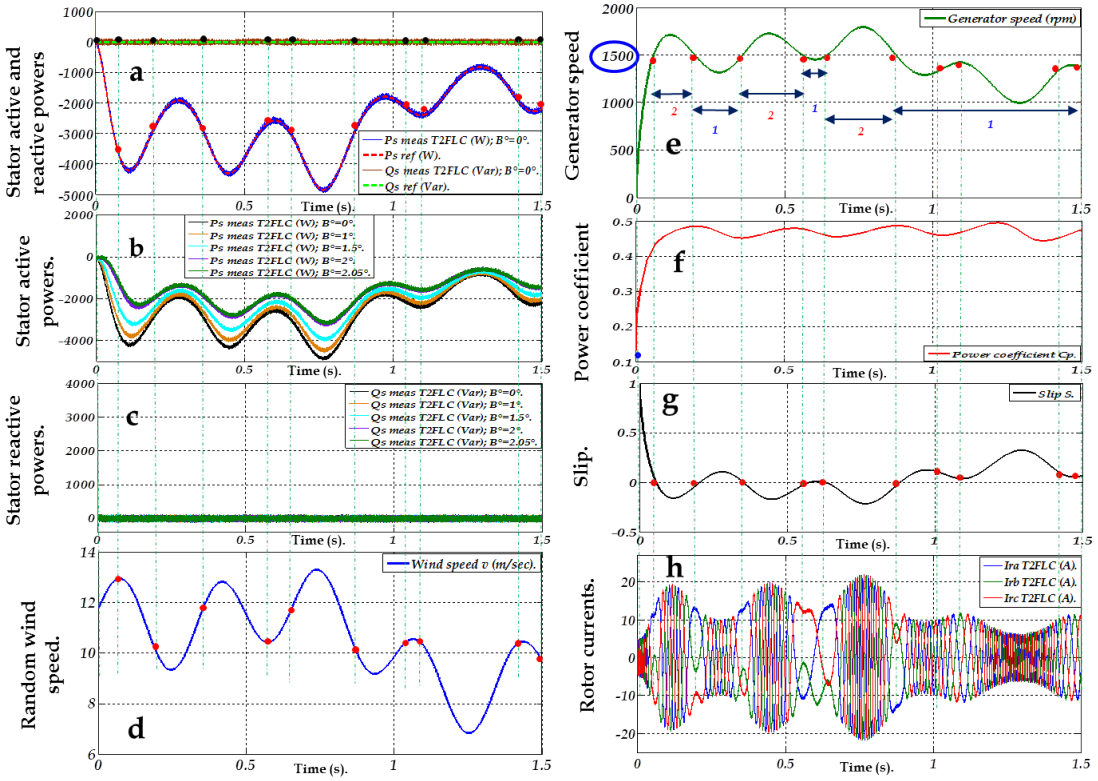

Fig. 12 (a) Stator active and reactive powers; (b) P_s under different $B°$ pitch angles; (c) Q_s under different pitch angles $B°$; (d) wind speed; (e) the generator speed; (f) power coefficient; (g) the slip; (h) the rotor currents

Table 4 A comparison of the proposed method with recently published control technologies

Ref.	Control technique	THD (%)	DFIG rated power	Overshoot	Dynamic response	Robustness
[5]	VGSTA-SMC	3.62	1.5 MW	Neglected	Fast	High
[7]	FOC-Hysteresis	3.5	3.5 KW	Neglected	Fast	Medium
[19]	IP-DPC	3.62	4.5 KW	Neglected	Excellent	High
[25]	ST-FOTSMC	---	2.0 MW	Neglected	Fast	---
[26]	Fuzzy SOSMC	0.28	1.5 MW	Neglected	Excellent	High
[27]	FOSMC	1.31	7.5 KW	----	----	Medium
[28]	Fuzzy DTC	1.73	1.5 KW	----	----	---
[29]	NDVC-FPWM	0.13	1.5 MW	Neglected	Fast	Medium
[30]	VM-DPC	1.7	2.0 MW	----	+++	---
[31]	Novel-FLC	---	10 MW	Neglected	Excellent	High
Proposed	T2-FLC	0.6	4 KW	Neglected	Excellent	High

7 Conclusion

In this paper, an adaptive T2-FLC for a wind energy conversion system based on a DFIG is presented. The T2-FLC is used to control the rotor d-q axis currents of the stator's active and reactive power in the rotor side converter. An SVM strategy is used to ensure a fixed switching frequency of the converters, and the MPPT approach is applied to ensure a unity power factor on the stator side. The performance of the T2-FLC has been investigated in both operating modes: Sub- and Super-synchronous. The simulation results obtained using MATLAB/Simulink® show high efficiency, low error, short response time, and dynamic power generation.

To further advance this research, the adaptive T2-FLC presented in this work offers significant potential for enhancing wind energy conversion systems. Future studies could focus on integrating this control strategy into advanced energy management systems for hybrid renewable sources, ensuring optimal energy distribution and improved grid stability. Experimental validation, including tests under fluctuating wind profiles and grid disturbances, is crucial to confirm the practical applicability of the proposed method. Moreover, it is recommended to integrate a Shunt Active Power Filter (SAPF) to enhance the quality of power injected into the load or micro-grid in future studies. Furthermore, extending the T2-FLC framework with robust control techniques, such as predictive control or higher-order sliding mode control, could enhance stability and resilience against uncertainties. Comparative studies with other intelligent control methods, such as fuzzy neural networks and reinforcement learning, would help identify the most effective approaches for specific applications. Additionally, evaluating performance under varying grid conditions and integrating energy storage systems could improve reliability and grid support capabilities. Scaling the T2-FLC methodology to other renewable energy systems, such as solar PV, or applying it in multi-agent systems for coordinated wind farm control, presents promising opportunities for innovation.

Nomenclature

WECS	Wind Energy Conversion System
WT	Wind Turbine
DFIG	Doubly-Fed Induction Generator
DFIM	Doubly-Fed Induction Motor
WRIG	Wound Rotor Induction Generator
IGBT	Insulated Gate Bipolar Transistor
PI	Proportional Integral
PVC	Power Vector Control
DPC	Direct Power control
MPDPC	Model Predictive Direct Power Control
INT-BCS	Integral Backstepping Controller
C-SMC	Conventional Sliding Mode Control
3O-SMC	Third Order Sliding Mode Control
T1FLC	Type-1 Fuzzy Logic Control
T2FLC	Type-2 Fuzzy Logic Control
THD	Total Harmonic Distortion
TSR	Tip Speed Ratio
PWM	Pulse Width Modulation
FIS	Fuzzy Inference System
VGSTA	Variable Gain Super Twisting Algorithm

References

[1] Itouchene, H., Amrane, F., Boudries, Z. "Robust Control of DFIG Wind Turbines in Sub/Super-Synchronous Operation Using Integral Backstepping Controller", Journal of Renewable Energies, 27(SI), pp. 23–31, 2024. https://doi.org/10.54966/jreen.v1i1.1170

[2] Amrane, F., Chaiba, A. "Improved Indirect Power Control (IDPC) of Wind Energy Conversion Systems (WECS)", Bentham Science Publishers, 2019, pp. 89–120. ISBN 978-981-14-1267-7 https://doi.org/10.2174/9789811412677119010l

[3] Amrane. F., Chaiba, A., Mekhilef S. "High performances of Grid-connected DFIG based on Direct Power Control with Fixed Switching Frequency via MPPT Strategy using MRAC and Neuro-Fuzzy Control", Journal of Power Technologies, 96(1), pp. 27–39, 2016. [online] Available at: https://papers.itc.pw.edu.pl/index.php/JPT/article/view/757 [Accessed: 01 January 2025]

[4] Global Wind Energy Council "Data & Analysis", [online] Available at: https://gwec.net/green-recovery-data-analysis/ [Accessed: 01 January 2025]

[5] Itouchene, H., Boudries, Z. Amrane, F. "Improved Power Control based Variable Speed Wind-Turbine DFIG under Hard Work Conditions: Application of Sliding Mode Theory", Periodica Polytechnica Electrical Engineering and Computer Science, 68(4), pp. 392–412, 2024. https://doi.org/10.3311/PPee.36760

[6] Cardenas, R., Pena, R., Alepuz, S., Asher, G. "Overview of Control Systems for the Operation of DFIGs in Wind Energy Applications", IEEE Transactions on Industrial Electronics, 60(7), pp. 2776–2798, 2013. https://doi.org/10.1109/TIE.2013.2243372

[7] Amrane, F., Chaiba, A., Babes, B. E., Mekhilef, S. "Design and Implementation of High Performance Field Oriented Control for Grid-connected Doubly Fed Induction Generator via Hysteresis Rotor Current Controller", Revue Roumaine des Sciences Techniques Serie Électrotechnique et Énergétique, 61(4), pp. 319–324, 2016. [online] Available at: http://revue.elth.pub.ro/index.php?action=details&id=609 [Accessed: 01 January 2025]

[8] Amrane, F., Chaiba, A. "A Hybrid Intelligent Control based on DPC for Grid-Connected DFIG with a Fixed Switching Frequency using MPPT Strategy", In: 2015 4th International Conference on Electrical Engineering (ICEE), Boumerdes, Algeria, 2015, pp. 1–4. ISBN 978-1-4673-6673-1 https://doi.org/10.1109/INTEE.2015.7416678

[9] Bourdoulis, M. K., Alexandridis, A. T. "Direct Power control of DFIG Wind Systems based On Nonlinear Modeling and Analysis", IEEE Journal of Emerging and Selected Topics in Power Electronics, 2(4), pp. 764–775, 2014. https://doi.org/10.1109/JESTPE.2014.2345092

[10] Hu, J., Zhu, J., Dorrell, D. G. "Predictive Direct Power Control of Doubly Fed Induction Generators Under Unbalanced Grid Voltage Conditions for Power Quality Improvement", IEEE Transactions on Sustainable Energy, 6(3), pp. 943–950, 2015. https://doi.org/10.1109/TSTE.2014.2341244

[11] Zarei, M. E., Nicolás, C. V., Arribas, J. R., Ramírez, D. "Four-Switch Three-Phase Operation of Grid-Side Converter of Doubly Fed Induction Generator With Three Vectors Predictive Direct Power Control Strategy", IEEE Transactions on Industrial Electronics, 66(10), pp. 7741–7752, 2019. https://doi.org/10.1109/TIE.2018.2880672

[12] Shehata, E. "Sliding Mode Direct Power Control of RSC for DFIGs Driven by Variable Speed Wind Turbines", Alexandria Engineering Journal, 54(4), pp. 1067–1075, 2015. https://doi.org/10.1016/j.aej.2015.06.006

[13] Beltran, B., Benbouzid, M. E. H., Ali, T. A. "Second-Order Sliding Mode Control of a Doubly Fed Induction Generator Driven Wind Turbine", IEEE Transactions on Energy Conversion, 27(2), pp. 261–269, 2012. https://doi.org/10.1109/TEC.2011.2181515

[14] Bossoufi, B., Karim, M., Lagrioui, A., Taoussi, M., Derouich, A. "Observer Backstepping Control of DFIG-Generators for Wind Turbines Variable-Speed: FPGA-Based Implementation", Renewable Energy, 81, pp. 903–917, 2015. https://doi.org/10.1016/j.renene.2015.04.013

[15] Ramesh, T., Panda, A. K., Kumar, S. S. "Type-2 Fuzzy Logic Control based MRAS Speed Estimator for Speed Sensorless Direct Torque and Flux Control of An Induction Motor Drive", ISA Transactions, 57, pp. 262–275, 2015. https://doi.org/10.1016/j.isatra.2015.03.017

[16] Ozsoy, E. E., Golubovic, E., Sabanovic, A., Gokasan, M., Bogosyan, S. "A Novel Current Controller Scheme for Doubly Fed Induction Generators", Automatika, 56(2), pp. 186–195, 2015. https://doi.org/10.7305/automatika.2015.07.766

[17] Evangelista, E., Puleston, P., Valenciaga, F., Dávila, A. "Variable gains super-twisting control for wind energy conversion optimi-zation", In: 2010 11th International Workshop on Variable Structure Systems (VSS), Mexico City, Mexico, 2010, pp. 50–55. ISBN 978-1-4244-5831-8 https://doi.org/10.1109/VSS.2010.5544713

[18] Deep, S., Sarkar, A., Ghawat, M., Rajak, M. K. "Estimation of the wind energy potential for coastal locations in India using the Weibull model", Renewable Energy, 161, pp. 319–339, 2020. https://doi.org/10.1016/j.renene.2020.07.054

[19] Amrane, F., Francois, B., Chaiba, A. "Experimental Investigation of Efficient and Simple Wind-Turbine based on DFIG-Direct Power Control using LCL-Filter for Stand-alone Mode", ISA Transactions, 125, pp. 631–664, 2022. https://doi.org/10.1016/j.isatra.2021.07.008

[20] Amrane, F., Francois, B., Chaiba, A. "Hardware Implementation study of Variable Speed Wind-Turbine-DFIG in Stand-alone Mode", In: 2020 22nd European Conference on Power Electronics and Applications (EPE'20 ECCE Europe), Lyon, France, 2020, pp. 1–8. ISBN 978-9-0758-1536-8 https://doi.org/10.23919/EPE20ECCEEurope43536.2020.9215946

[21] Amrane, F., Chaiba, A., Francois, B., Babes, B. E. "Experimental design of stand-alone field oriented control for WECS in variable speed DFIG-based on hysteresis current controller", In: 2017 15th International Conference on Electrical Machines, Drives and Power Systems ELMA, Sofia, Bulgaria, 2017, pp. 304–308. ISBN 978-1-5090-6691-9 https://doi.org/10.1109/ELMA.2017.7955453

[22] Amrane, F., Chaiba, A., Francois, B. "Suitable power control based on type-2 fuzzy logic for wind-turbine DFIG under Hypo-synchronous mode fed by multi-level converter", In: 2017 5th International Conference on Electrical Engineering - Boumerdes (ICEE-B), Boumerdes, Algeria, 2017, pp. 1–6. ISBN 978-1-5386-0686-5
https://doi.org/10.1109/ICEE-B.2017.8191983

[23] Amrane, F., Chaiba, A., Francois, B., Babes, B. E. "Real time implementation of grid-connection control using robust PLL for WECS in variable speed DFIG-based on HCC", In: 2017 5th International Conference on Electrical Engineering - Boumerdes (ICEE-B), Boumerdes, Algeria, 2017, pp 1–5. ISBN 978-1-5386-0686-5
https://doi.org/10.1109/ICEE-B.2017.8191984

[24] Amrane, F., Chaiba, A., Francois, B. "Improved Adaptive Nonlinear Control for Variable Speed Wind-Turbine fed by Direct Matrix Converter", Revue Roumaine des Sciences Techniques Serie Électrotechnique et Énergétique, 68(1), pp. 58–64, 2023.
https://doi.org/10.59277/RRST-EE.2023.68.1.10

[25] Irfan, S., Shafaat, U., Zahoor, A., Nasim, U., Jong-Suk, R. "A Super Twisting Fractional Order Terminal Sliding Mode Control for DFIG-Based Wind Energy Conversion System", Energies, 13(9), 2158, 2020.
https://doi.org/10.3390/en13092158

[26] Alhato, M. M., Bouallègue, S., Rezk, H. "Modeling and Performance Improvement of Direct Power Control of Doubly-Fed Induction Generator Based Wind Turbine through Second-Order Sliding Mode Control Approach", Mathematics, 8(11), 2012, 2020.
https://doi.org/10.3390/math8112012

[27] Beniss, M.A., El Moussaoui, H., Lamhamdi, T., El Markhi1, H. "Improvement of power quality injected into the grid by using a FOSMC-DPC for doubly fed induction generator", International Journal of Intelligent Engineering & Systems, 14(2), pp. 556–567, 2021.
https://doi.org/10.22266/ijies2021.0430.50

[28] El Ouanjli, N., Motahhir, S., Derouich, A., El Ghzizal, A., Chebabhi, A., Taoussi, M. "Improved DTC strategy of doubly fed induction motor using fuzzy logic controller", Energy Reports, 5, pp. 271–279, 2019.
https://doi.org/10.1016/j.egyr.2019.02.001

[29] Benbouhenni, H., Bizon, N. "Advanced Direct Vector Control Method for Optimizing the Operation of a Double-Powered Induction Generator-Based Dual-Rotor Wind Turbine System", Mathematics, 9(19), 2403, 2021.
https://doi.org/10.3390/math9192403

[30] Peng, C., Chao, W., Fuwei, N., He, J. "Voltage Modulated DPC Strategy of DFIG Using Extended Power Theory under Unbalanced Grid Voltage Conditions", Energies, 13(22), 6077, 2020.
https://doi.org/10.3390/en13226077

[31] Phung, B. N., Wu, Y.-K., Pham, M.-H. "Novel Fuzzy Logic Controls to Enhance Dynamic Frequency Control and Pitch Angle Regulation in Variable-Speed Wind Turbines", Energies, 17(11), 2617, 2024.
https://doi.org/10.3390/en17112617

Appendix

Table A1 Parameters of the DFIG

Parameters	Values
Rated power	4.0 kW
Stator resistance	$R_s = 1.2\ \Omega$
Rotor resistance	$R_r = 1.8\ \Omega$
Stator inductance	$L_s = 0.1554$ H.
Rotor inductance	$L_r = 0.1558$ H.
Mutual inductance	$L_m = 0.15$ H.
Rated voltage	$V_s = 220/380$ V
Number of pole pairs	$p = 2$
Rated speed	$N = 1440$ rpm
Friction coefficient	$f_{DFIG} = 0.00$ N.m/sec
The moment of inertia	$J = 0.2$ kg.m^2

Table A2 Parameters of the turbine

Parameters	Values
Rated power	4.5 kW
Number of blades	$P = 3$
Blade diameter	$R = 3$ m
Gain	$G = 4.15$
The moment of inertia	$J_t = 0.00065$ kg.m^2
Friction coefficient	$f_t = 0.017$ N.m/sec
Air density	$\rho = 1.22$ Kg/m^3